Complex evolution of the electronic structure from polycrystalline to monocrystalline graphene: Generation of a new Dirac point

Joice da Silva Araújo and R. W. Nunes*
Departamento de Física, Universidade Federal de Minas Gerais, CP 702, Belo Horizonte 30123-970, MG, Brazil
(Received 17 November 2009; revised manuscript received 20 January 2010; published 23 February 2010)

First principles calculations, employed to address the properties of polycrystalline graphene, indicate that the electronic structure of tilt grain boundaries in this system displays a rather complex evolution toward graphene bulk, as the tilt angle decreases, with the generation of a Dirac point, at the Fermi level, that lies not on the usual graphene Brillouin zone **K** point, and an anisotropic Dirac cone of low-energy excitations. Moreover, the usual **K**-point Dirac cone falls below the Fermi level, and rises toward it as the tilt angle decreases. Further, our calculations indicate that the grain-boundary formation energy behaves nonmonotonically with the tilt angle, due to a change in the spatial distribution and relative contributions of the bond-stretching and bond-bending deformations associated with the formation of the defect.

DOI: 10.1103/PhysRevB.81.073408 PACS number(s): 73.22.−f, 68.65.−k

Graphene—an isolated layer of sp^2-bonded carbon atoms arranged in a honeycomb structure—was until very recently, a "theoretical" reference system for the study of the properties or the "real" sp^2-bonded carbon forms, such as fullerenes, nanotubes, and graphite.[1–4] Since the recent report of the isolation of a stable single-atom-thick carbon layer, by exfoliation of graphite,[5] graphene itself has occupied the center stage of Materials Physics, as a paradigmatic system for "relativistic" condensed-matter phenomena, as well as a promising material for Nanoelectronics, due to its exceptional electronic properties. Graphene is a null-gap semiconductor with a vanishing density of states at the Fermi level, and electronic bands that are linear and isotropic within ~1 eV from the Fermi level. This linearity and the presence of two sublattices imply that charge carriers in graphene effectively behave as massless chiral "relativistic" particles, being described by Dirac's equation.[1,2,4] Due to the chiral nature of the electronic excitations, which leads to the absence of backscattering, graphene holds ballistic charge transport on the microscale, even at room temperature, and with high concentrations of defects and impurities.[1,2,5,6] In the last few years, scientific interest in graphene has rapidly intensified, and the material is expected to play a major role in Nanoelectronics in the future.

Presently, common synthesis routes for graphene are the original exfoliation method,[5] that produces monocrystalline graphene samples, and epitaxy, mostly on SiC[7] and metallic substrates.[8] Recent works on epitaxially-grown graphene report the occurrence of superstructures interpreted as Moiré patterns[9,10] based on scanning tunneling microscopy (STM), atomic force microscopy (AFM), and scanning tunneling spectroscopy (STS) measurements. Moiré patterns and superstructures, associated with layer stacking, as well as the occurrence of bulk and surface grain boundaries (GBs), are topics of prominence in the physics of highly oriented pyrolytic graphite (HOPG) itself.[11–15] GBs are among the most commonly occurring extended defects in HOPG, because of its polycrystalline character.[15] For large scale graphene production and application, it is expected that synthesis methods will be epitaxy based, being quite conceivable that polycrystalline samples will be produced. Indeed, the occurrence of GBs on the graphene layer has been recently reported,[9] speculated as a probable source of long-range electronic perturbations in graphene on SiO_2,[10] and further, the lower carrier mobility of epitaxial graphene (when compared with exfoliated samples), in a macroscopic-size graphene field-effect transistor, has been tentatively assigned to the electronic perturbations associated with GBs.[16]

Previous works have addressed the electronic properties of disordered graphene, but these have focused on the effects of point defects, corrugation, and extended edge states in graphene ribbons, drawing only speculative conclusions in what regards the electronic states of GBs.[1] In this scenario, addressing properties of GBs in graphene is of primary relevance. In the present work, we employ first principles calculations to examine the energetics and electronic properties of GBs in graphene. We focus on the structural GB model proposed by Simonis *et al.*,[11] who observed a large-angle tilt boundary on the surface of HOPG, on STM experiments. These authors proposed that, in the absence of stress, the observed GB consists of a periodic structure that can be described as a regular succession of pentagon-heptagon pairs, as shown in Fig. 1. Based on this model, we investigate three GBs of different periodicities along the boundary, hence with different relative orientation between the grains.

We find that, while large-angle tilt GBs do not introduce localized states at the Fermi level in graphene, various resonance peaks appear in the density of states of the material, over a broad energy range, starting at energies of ~0.3 eV

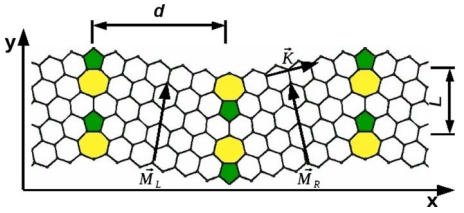

FIG. 1. (Color online) Grain boundary geometry: the relative orientation between grains is defined by the angle between vectors $\vec{M}_L$ and $\vec{M}_R$. The distance between the two grain boundaries in the supercell is d, and L is the period of the pentagon-heptagon pattern along the grain boundary.

from the Fermi level, in agreement with recent experimental work.[15] More importantly, the changes in electronic structure with the GB tilt angle indicate a nontrivial evolution toward graphene bulk, as the GB angle decreases: we observe the generation of a Dirac point at the Fermi level, which lies on a line that evolves toward the Γ-**M** direction of the graphene Brillouin zone (BZ), with the usual Dirac point at the **K** point falling below the Fermi level, and rising toward it as the tilt angle decreases. The Dirac cone of low-energy excitations around the Dirac point at the Fermi level is nonisotropic, with the effective "speed-of-light" depending on the direction in the BZ away from the Dirac point. Furthermore, our calculations indicate that, within the structural model we consider, the GB formation energy does not behave monotonically with the period of the GB (or, equivalently, with the tilt angle). A Keating analysis of the elastic energy, associated with the formation of the defect, indicates that a change in the spatial distribution and relative contributions of the stretching and bending deformations leads to the nonmonotonicity indicated by our results.

All calculations are performed using Kohn-Sham density functional theory,[17] the generalized-gradient approximation (GGA)[18] for the exchange-correlation term, and norm-conserving Troullier-Martins pseudopotentials,[19] to describe the electron-ion interaction. We use the linear combination of atomic orbitals (LCAO) method implemented in the SIESTA code,[20] with a double-zeta pseudoatomic basis set plus polarization orbitals, with an energy cutoff of 0.01 Ry. Structural optimization is performed until the total force on each atom is less than 0.02 eV/Å. In order to simulate an isolated honeycomb sheet, we use supercells that are periodic along the graphene plane, and are surrounded by a 33 Å vacuum region, such that the interactions between each layer and its periodic images are negligible.

Periodicity along the graphene plane requires the supercell to contain two GBs of opposite tilt angles (a GB and the corresponding "anti-GB"), as shown in Fig. 1 for the GB1 geometry. The experimental value in Ref. 11 for the relative orientation between grains is 21°, defined here by the angle α between vectors $\vec{M}_L$ and $\vec{M}_R$, drawn respectively on the left and right grains adjacent to the GB, as shown in Fig. 1. This model can be extended to GBs with smaller tilt angles, by adding lines of hexagons, such that the period L of the pentagon-heptagon pattern along the GB increases. In the $L\rightarrow\infty(\alpha\rightarrow 0)$ limit, we recover the perfect single-crystal graphene lattice. We study three different GB geometries, with the theoretical values for L and α indicated in Table I. GB1 is the model proposed in Ref. 11, with $\alpha=21.8°$ and $L=6.6$ Å; GB2 has $\alpha=13.3°$ and $L=10.9$ Å; and for GB3 $\alpha=9.6°$ and $L=15.2$ Å. In order to ensure that we simulate the properties of an isolated GB, we consider supercells with increasing distances d between the GBs and their periodic images. Formation energy results are converged for $d=14.9$ Å. The geometric parameters α, d, and L are shown in Fig. 1, with values for α and L given in Table I.

The band-structure of the GB1 ($\alpha=21.8°$), is shown in Fig. 2(a). The Brillouin zone for this GB supercell is shown in Fig. 3(b). The Γ-**Y** direction is along the GB, and the Γ-**X** direction is perpendicular to it. In Fig. 3(b), we also indicate lines we denoted as Γ-**M** and Γ-**K**, which correspond to these high-symmetry directions in a single-crystal graphene sheet with the orientation of the grain on the right side of the GB. Γ-**M** (and Γ-**Y**) and Γ-**K** (and Γ-**X**) converge to the corresponding directions in the $\alpha\rightarrow 0$ limit, where a single-crystal graphene sheet is recovered. A mirror plane, perpendicular to the graphene sheet and through the geometric center of the GB, relates the Γ-**M** and Γ-**K** lines of the two adjacent grains. Note that the Fermi level or Dirac point occurs on the Γ-**Y** line, in the point marked as D in Fig. 3(b), and that band crossings, which lie below the Fermi level, occur at the **X** and **K** points.

TABLE I. Geometric parameters and formation energy per unit length E_f (in eV/Å), of GB supercells containing N_a atoms. α is the tilt angle and L is the GB period (in Å), as indicated in Fig. 1. E_{el}^{str} and E_{el}^{bend} are the contributions to the Keating-model total elastic energy per unit length E^{el}

	N_a	α (°)	L	E_f	E_{el}	E_{el}^{str}	E_{el}^{bend}
GB1	72	21.8	6.6	0.33	0.42	0.10	0.32
GB2	120	13.3	10.9	0.42	0.47	0.15	0.31
GB3	168	9.6	15.2	0.40	0.41	0.15	0.27

Thus, we observe the generation of a Dirac cone,[21] on the Γ-**Y** direction, which is anisotropic, with a Fermi velocity (the effective "velocity of light") that depends on the direction from the Dirac point in **k** space. This Dirac cone is shown in Fig. 3(a), for the region around the **D** point indicated in Fig. 3(b). The energy isolines are shown Fig. 3(c), where the anisotropy of the cone is clearly displayed: the more (less) elongated is the isoline along a given direction, the smaller (larger) is the Fermi velocity along that direction. The band-structures for the GB2 ($\alpha=13.3°$) and GB3 ($\alpha=9.6°$) are shown in Figs. 2(b) and 2(c), respectively. Note again the occurrence of a Dirac point at the Fermi level, on the Γ-**Y** line, in both cases. Both display anisotropic Dirac cones as well. The isolines for the GB3, shown in Fig. 3(d), are less anisotropic than in the GB1 case. In Table II we

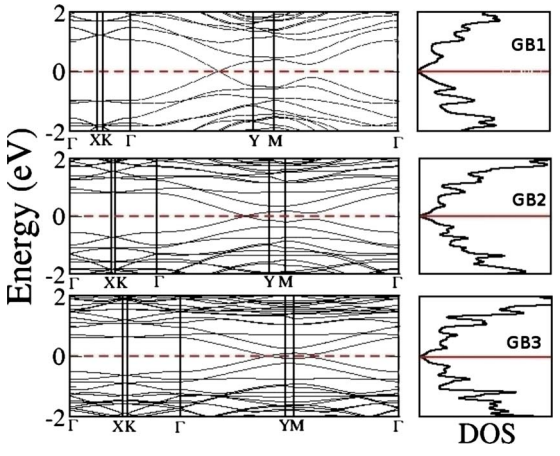

FIG. 2. (Color online) Band structure and density of states for (a) GB1, (b) GB2, and (c) GB3 geometries. The Fermi level is indicated by the dashed line. Brillouin-zone lines are shown in Fig. 3.

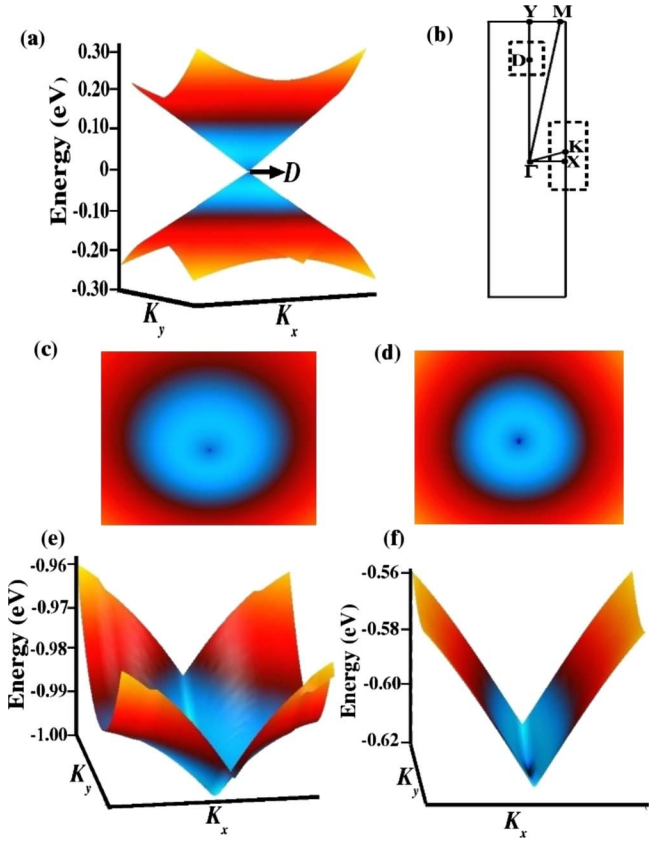

FIG. 3. (Color online) Electronic energy dispersion for polycrystalline graphene. (a) The anisotropic Dirac cone around the **D** point, for the GB1. (b) The Brillouin-zone directions and regions for the GB1. (c) and (d) The color-coded constant-energy isolines (with the energy increasing from violet to red) for the GB1 and GB3, respectively. (e) and (f) The wedge-shaped dispersion around the **K**-**X** line shown in (b).

include the Fermi velocities for the Dirac cones of the three GBs, along the indicated directions.

A comment is in order regarding the occurrence of Dirac cone in the pollycrystaline graphene models we consider. The above mentioned mirror symmetries are related to the Dirac point degeneracies, as indicated by calculations with poorer **k**-point sampling, for which we observe the opening of rather small (~ 8 meV) gaps at the Dirac point, related to the numerical symmetry breaking due to the poorly converged **k**-space sums. This is further confirmed by calculations where the mirror symmetry was imposed by geometrical constraints, for which the gaps vanished and the crossings were recovered, even with unconverged **k**-point sampling. In our **k**-point-sampling-converged calculations, the single-particle energy eigenvalues are numerically converged to better than 1 meV.

TABLE II. Fermi velocities (in 10^6 m/s) for the GB Dirac electron cones, along the indicated directions.

	$-\hat{y}$	$-(\hat{x}+\hat{y})$	$-\hat{x}$	$\hat{x}$	$\hat{x}+\hat{y}$	$\hat{y}$
GB1	0.73	0.69	0.60	0.60	0.52	0.50
GB2	0.64	0.59	0.52	0.52	0.48	0.42
GB3	0.55	0.53	0.57	0.57	0.54	0.45

The nature of the electronic dispersion in the region around the **X** and **K** points, also indicated in Fig. 3(b), are shown in Figs. 3(e) and 3(f), for the GB1 and GB3, respectively. For the GB3, there is very little dispersion along the **X**-**K** direction, resulting in a straight wedge cutting through this line, while in the GB1, the shape of the energy dispersion is also wedgelike, but a "flowery" shape develops at higher energies. Furthermore, the band crossings at the **X** and **K** points move up toward the Fermi level, as α decreases, which is consistent with the $\alpha \rightarrow 0$ limit, where the Fermi level occurs at the **K** point. The energy difference between the Dirac point at **D** and the **K** point is 1.00 eV for the GB1, 0.73 eV for the GB2, and 0.64 eV for the GB3.

These results indicate a very complex evolution of the band structure of polycrystalline graphene with the GB angle. Since fivefold and sevenfold topological defects constitute the core of low-energy dislocations in graphene,[22] they are probably ubiquitous in any realistic model of GBs in this material. Hence, the occurrence of a Dirac point along the GB direction may prove a robust feature of polycrystalline graphene. We note that previous works have found that, while pentagon-heptagon pairs and the related SW defect introduce no resonant states *at the Dirac point* in graphene, resonance peaks appear in the density of states starting at a few tenths of an eV from the Fermi level, a result that we have also reproduced with the *ab initio* method employed here. Our GB electronic structure calculations show, however, that the periodic superstructure formed by these dislocations along the GB line shares with perfect graphene the vanishing gap and the Dirac-like nature of electronic excitations, but in a rather complex structure, with direction-dependent Fermi velocities, the generation of a Fermi-level Dirac point along the GB direction, and a wedge-like dispersion around the **K** point that should evolve toward the graphene Dirac cone as $\alpha \rightarrow 0$. We expect charge transport in polycrystalline graphene to reflect the anisotropic structure of the Dirac cones we obtain in our calculations.

We turn now to the GB energetics. The GB formation energy per unit length is given by $E_f=(E_{GB}-E_{bulk})/2L$, where E_{GB} and E_{bulk} are the calculated total energies of the GB and bulk graphene supercells, respectively. The factor of two on the right-hand side accounts for the presence of two GBs in the cell.

Results in Table I show that E_f varies nonmonotonically with the GB period. Among the three GBs, GB1 with a tilt angle of 21.8° has the smallest formation energy, while GB2 with $\alpha=13.3°$ has the highest E_f value. We expect that $E_f \rightarrow 0$ as $\alpha \rightarrow 0$. Our results indicate that E_f initially increases, before reaching this asymptotic limit. Given the absence of broken bonds in the GB geometries, E_f is primarily of elastic nature. In order to understand this nonmonotonic behavior, we use a Keating model to analyze the bond-bending E_{el}^{bend}, and bond-stretching E_{el}^{str} contributions to the GB elastic energy E_{el}. The results are shown in Table I. For the GB1 we observe that E_{el}^{bend} is a factor of 3.2 larger than E_{el}^{str}, while for the GB2 and GB3 structures the $E_{el}^{bend}/E_{el}^{strch}$ ratio decreases to 2.1 and 1.8, respectively. These results remain essentially unaltered for different choices of the ratio

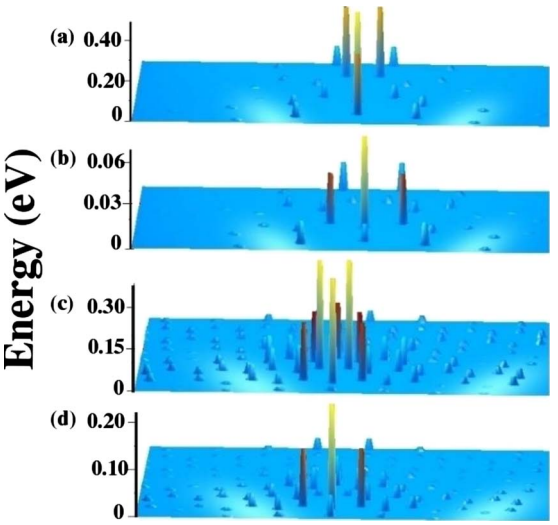

FIG. 4. (Color online) Spatial distribution of bond-bending and bond-stretching energies of grain boundaries in graphene. (a) Bend for GB1. (b) Stretch for GB1. (c) Bend for GB3. (d) Stretch for GB3.

between the stretching and bending energy parameters of the Keating model. Moreover, the spatial distribution of E_{el}^{bend} and E_{el}^{strech} changes as α decreases, as shown in Fig. 4. For the GB1, E_{el}^{bend} is largely concentrated on the atoms at the very core of the boundary, mainly in the pentagon-heptagon pairs, while E_{el}^{str} is a little more spread out toward the interior of the grains. For GB3, we see that both E_{el}^{bend} and E_{el}^{str} have significant contributions from atoms in the interior of the grain, mostly on the hexagon lines that end at the pentagon-heptagon at the boundary. Thus, by concentrating the elastic energy on bending distortions at the defect core, the GB1 structure relaxes to a lower energy state than GBs with smaller angles, which leads to the nonmonotonic behavior of E_f.

To conclude, *ab initio* calculations indicate that the electronic structure of tilt GBs in graphene display a complex evolution toward graphene bulk, as the GB angle decreases, with the generation of a Dirac point at the Fermi level, that lies on a line that evolves toward the Γ-**M** direction of the graphene Brillouin zone. This Dirac point is the vertex of an anisotropic electronic-energy cone. Moreover, the usual Dirac point at the **K** point falls below the Fermi level, and rises toward it as the tilt angle decreases. Furthermore, our calculations indicate that the GB formation energy behaves non-monotonically with the tilt angle, due to a change in the spatial distribution and relative contributions of the bond-stretching and bond-bending deformations associated with the formation of the defect.

ACKNOWLEDGMENTS

We acknowledge support from the Brazilian agencies CNPq, FAPEMIG, Rede de Pesquisa em Nanotubos de Carbono, INCT de Nanomateriais de Carbono, and Instituto do Milênio em Nanotecnologia-MCT.

*rwnunes@fisica.ufmg.br

[1] A. H. Castro Neto, F. Guinea, N. M. R. Peres, K. S. Novoselov, and A. K. Geim, Rev. Mod. Phys. **81**, 109 (2009) and references therein.
[2] A. K. Geim and K. S. Novoselov, Nature Mater. **6**, 183 (2007).
[3] K. Nakada, M. Fujita, G. Dresselhaus, and M. S. Dresselhaus, Phys. Rev. B **54**, 17954 (1996).
[4] P. R. Wallace, Phys. Rev. **71**, 622 (1947).
[5] K. S. Novoselov, A. K. Geim, S. V. Morozov, D. Jiang, Y. Zhang, S. V. Dubonos, I. V. Grigorieva, and A. A. Firsov, Science **306**, 666 (2004).
[6] M. I. Katsnelson, K. S. Novoselov, and A. K. Geim, Nat. Phys. **2**, 620 (2006).
[7] C. Berger, Z. M. Song, T. B. Li, X. B. Li, A. Y. Ogbazghi, R. Feng, Z. T. Dai, A. N. Marchenkov, E. H. Conrad, P. N. First, and W. A. de Heer, J. Phys. Chem. B **108**, 19912 (2004); J. Hass, R. Feng, J. E. Millan-Otoya, X. Li, M. Sprinkle, P. N. First, W. A. de Heer, E. H. Conrad, and C. Berger, Phys. Rev. B **75**, 214109 (2007).
[8] O. V. Sinitsyna and I. V. Yaminsk, Russ. Chem. Rev. **75**, 23 (2006).
[9] L. B. Biedermann, M. L. Bolen, M. A. Capano, D. Zemlyanov, and R. G. Reifenberger, Phys. Rev. B **79**, 125411 (2009).
[10] S. S. Datta, D. R. Strachan, E. J. Mele, and A. T. C. Johnson, Nano Lett. **9**, 7 (2009).
[11] P. Simonis, C. Goffaux, P. A. Thiry, L. P. Biro, P. Lambin, and V. Meunier, Surf. Sci. **511**, 319 (2002).
[12] Y. Gan, W. Chu, and L. Qiao, Surf. Sci. **539**, 120 (2003).
[13] W.-T. Pong, J. Bendall, and C. Durkan, Surf. Sci. **601**, 498 (2007).
[14] F. Varchon, P. Mallet, L. Magaud, and J.-Y. Veuillen, Phys. Rev. B **77**, 165415 (2008).
[15] J. Červenka and C. F. J. Flipse, Phys. Rev. B **79**, 195429 (2009).
[16] G. Gu, S. Nie, R. M. Feenstra, R. P. Devaty, W. J. Choyke, W. K. Chan, and M. G. Kane, Appl. Phys. Lett. **90**, 253507 (2007).
[17] W. Kohn and L. J. Sham, Phys. Rev. **140**, A1133 (1965).
[18] L. Kleinman and D. M. Bylander, Phys. Rev. Lett. **48**, 1425 (1982).
[19] N. Troullier and J. L. Martins, Phys. Rev. B **43**, 1993 (1991).
[20] J. M. Soler, E. Artacho, J. D. Gale, A. Garcia, J. Junquera, P. Ordejon, and D. Sanchez-Portal, J. Phys.: Condens. Matter **14**, 2745 (2002).
[21] C. H. Park, L. Yang, Y. W. Son, M. L. Cohen, and S. G. Louie, Phys. Rev. Lett. **101**, 126804 (2008).
[22] A. Carpio, L. L. Bonilla, F. de Juan, and M. A. H. Vozmediano, New J. Phys. **10**, 053021 (2008).